Joint PA and FDA Beamforming for Radar-Communications Systems

Freddy Y.P. Feng, Suk Chan Kim, Ziming He, Feng Chen, Chen Lu, Sami Muhaidat

***Abstract*—Integrated wireless communications and Radar detections have so far mainly relied on phased-array (PA) antennas with only considering the beampatterns in angle domain. In this paper, by taking advantage of frequency diverse array (FDA), which can generate beampatterns in angle, range and time domains, we propose a novel finite orthogonal random FDA, whose beampatterns feature periodical pulses in time or range domain. By applying this technology into Radar and communications (RadComm) systems, a compact dual-functional structure of joint PA and FDA is designed. With the proposed novel structure, the common information, such as channel status information and direction-of-arrival can be easily shared for both PA communications and FDA Radar. Based on the built joint PA and FDA channel models, different beamformer designs are proposed by jointly optimizing the signal-to-interference-noises of the communications and Radar. In addition, we robustify the proposed method by considering the case of channel estimation imprecision. Numerical simulations demonstrate the performances of both communications and the Radar with the proposed approaches are over than that of the conventional PA RadComm systems.**

***Index Terms*—Radar and Communication, frequency divers array, joint PA and FDA, finite orthogonal random.**

I. Introduction

RESPOND to the explosive growth of wireless communications devices and the rapidly increasing demand for free frequency spectrum, co-existence between Radar and communications (RadComm) over shared bandwidths has been put forward as a challenging topic in recent years.

The pioneering work named null space projection (NSP) was proposed [1] for the coexistence of MIMO Radar and communications, in which the designed Radar beamformer is in the null space of the interference channel between the Radar and base station (BS) so that no cross interference can be imposed on the communications and Radar systems. Based on this approach, [2]–[5] concentrate on investigating different trade-offs between the performance of Radar and communications by relaxing the zero-forcing precoder as the projection matrix. In [6], by exploiting the multi-user interference (MUI) as a useful source of transmission power, an approach is suggested to trade off the quality of the beampattern and downlink signal-to-interference-noise ratio (SINR). [7] considers joint transmit and receive beamformers for both MIMO Radar and MIMO communications systems and designs a two-tier alternating optimization spectrum sharing framework based on interference alignment approach. In [8], a sparsity-aware beamforming design is put forward, which permits a trade-off between communications rate and Radar detection performance in the angular domain. This method uses random transmit antenna subsets to form a coherent beam towards a communications receiver while simultaneously perturbing the sidelobes of the resulting beampattern. Generally, the works mentioned above all employ the traditional phased array (PA) for the Radar and communications.

In recent years, the field of radar-communication (RadComm) integration has seen significant advancements, with Frequency Diverse Array (FDA) technology emerging as a promising solution to address the limitations of traditional phased arrays [9]–[15]. FDA offers unique capabilities in generating beams simultaneously in angle, range, and time domains, providing enhanced spatial resolution and range-dependent beamforming [16]–[25].

Unlike conventional phased arrays, which generate only angle-dependent beams, FDA introduces small frequency offsets to array elements, resulting in a range-angle-dependent beampattern [9], [10]. This characteristic enables FDA to distinguish signals from different range cells, offering significant advantages in various applications, including deceptive jamming suppression [9], moving target deception [10], and enhanced target estimation [12].

Recent studies have focused on optimizing FDA beampattern synthesis to achieve better performance. For instance, Wang et al. [11] proposed a random permutated power increasing frequency offset scheme (RP-Pow-FDA) to achieve lower sidelobe levels and improved anti-noise performance. Similarly, [12] introduced a particle swarm optimization approach for frequency offset design, resulting in a dot-shaped transmit beampattern with better time-invariant performance.

The versatility of FDA extends beyond linear array geometries. [13] explored discular FDA (DFDA) to achieve true 3D dot-shaped beamforming, expanding the potential applications of FDA in spatial energy focusing. Furthermore, innovative implementations such as the mirrored two-wave mixing FDA proposed by Yang et al. [14] offer low-cost solutions for FDA realization, potentially broadening its adoption in practical systems.

In the context of emerging technologies, FDA has shown

This work is support by Shenzhen Municipal Commission of Science and Technology Innovation with the grant funding numbers of 20220818232202001 and GJHZ20220913143013024.

Freddy Y.P. Feng and Chen Lu are with the College of Information and Communications, Shenzhen Institute of Information Technology, Shenzhen, China (e-mail: freddy.yp.feng@gmail.com, luchen@sziit.edu.cn).

Suk Chan Kim (*Corresponding author*) is with the Department of Electronics Engineering, Pusan National University, Busan 46241, South Korea (e-mail: sckim@pusan.ac.kr).

Z. He and F. Chen are with Zhejiang Vie Science & Technology Co., Ltd, Zhejiang, China (e-mail: heziming.vie@gmail.com, mervyn@vie.com.cn).

S. Muhaidat is with Khalifa University, Abu Dhabi, United Arab Emirates (e-mail: sami.muhaidat@ku.ac.ae).

promise in enhancing wireless power transfer for Internet of Things (IoT) devices. Lee et al. [15] developed a dynamic energy beamforming scheme using FDA, demonstrating improved energy harvesting performance for multiple IoT devices simultaneously. However, FDA beampattern is time-varying and most the works only consider a special time, i.e., $t = 0$.

In this work, we propose a novel finite orthogonal random (FOR) FDA scheme, which can generate a period pulsed beampattern, and apply it into the RadComm system to reduce the overlapped radio resource blocks, such as time and frequency. The main contributions of this work are listed as follows:

1) Propose a module structure for the joint PA and FDA RadComm system. Through the shared antenna array, the PA and FDA are combined into one system, where some common information can be shared directly, such as the estimations of channel status information (CSI), the direction-of-arrival (DOA) and data.

2) Establish the joint PA and FDA channel model. For simplicity, this article only considers the geometric MIMO channel model, although other channel models can also be extended. Based on the proposed joint PA and FDA structure, the wireless channel model between PA and FDA is derived, where the part of the channel from FDA to clusters is featured by the FDA steering vectors while the rest part from the clusters to the mobile station (MS)is characterized by multiple conventional PA steering vectors.

3) Design the joint PA and FDA beamformers. By jointly optimizing the SINR of communications and the Radar, we proposed two algorithms to obtain the beamformers of the Radar and communications, which are named ratio-maximizing approach and quadratically constrained quadratic programming (QCQP) approach.

4) Robustify the proposed method. Considering the problem of channel estimation imprecision, we proposed a theorem to guarantee the proposed method works in a given value of probability.

5) Design the pulse waveform of FOR-FDA signal. By studying a bi-frequency periodical FDA, we find out the method to control the parameters of the proposed FOR-FDA pulse, such as pulse period, pulse width in both time and angle domains.

The rest of the paper is organized as follows. Section II provides a brief background of FDA and the motivation of this article. Section III proposes the architecture of the joint PA and FDA dual-function system, in which the joint PA and FDA module architecture and system model are described. Section IV addresses the optimization problems of joint beamforming. Section V discusses the robustness of the proposed method. Section VI gives the numerical simulations, where the joint SINR of RadComm, convergence rate and complexity are discussed. Finally, we conclude this article in Section VII.

II. Background and Motivation

The carrier frequences for the PA are same for all the RF chains and the beampattern only depends on its angle, while the carrier frequencies for the FDA are non-identical for all the RF chains and the beampattern associates with the range, angle and time, simultaneously.

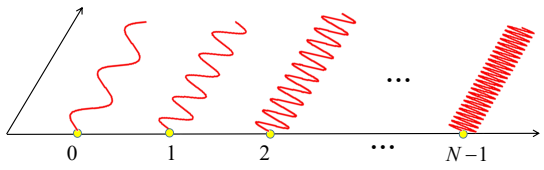

Fig. 1: Structure of FDA.

Without loss of generality, we consider the uniform linear array (ULA) as shown in Fig. 1. For an N-element ULA, the waveform transmitted by the nth element at the time t can be represented by

$$\tilde{s}_n(t) = \exp\{j2\pi(f_0 + \Delta f_n)t\}, \tag{1}$$

where f_0 is the basic carrier frequency and Δf_n ($\ll f_0$) denotes the frequency offset of the nth antenna.

The transmitted signal from the nth element arriving at a far-field position can be written as

$$\begin{aligned} s_n(\theta, r_0, t) = &\exp\{j2\pi f_0(t - r/c_0)\} \\ &\cdot \exp\{j2\pi(nf_0 d\sin\theta/c_0 - \Delta f_n r/c_0 + \Delta f_n t)\}. \end{aligned} \tag{2}$$

where θ is the direction-of-arrival (DOA), r denotes the distance between the first antenna and the field position, $r_n \approx r - nd\sin\theta$ denotes the distance from the n-th element to the field position, c_0 is the light speed, and d is the inter-element space. Since $\Delta f_n \ll f_0$, we have $2\pi\Delta f_n d\sin\theta/c_0 \approx 0$.

For the standard FDA, the frequency offset for each antenna linearly increases along with antenna elements, i.e., $\Delta f_n = nf_d$, where $f_d \ll f_0$ is a constant frequency step size. Assume the uniform weighs are adopted, i.e., $w_n = 1$, the FDA beampattern can be synthesized as

$$\begin{aligned} P(\theta, r, t) = &\exp\{j2\pi f_0(t - r/c_0)\}\cdot \\ &\sum_{n=0}^{N-1} \exp\{jn2\pi(f_0 d\sin\theta/c_0 - f_d r/c_0 + f_d t)\}. \end{aligned} \tag{3}$$

Then, the amplitude of the beampattern can be formulated as

$$|P(\theta, r, t)| = \left|\frac{\sin[\pi N(f_0 d\sin\theta/c_0 - f_d r/c_0 + f_d t)]}{\sin[\pi(f_0 d\sin\theta/c_0 - f_d r/c_0 + f_d t)]}\right|. \tag{4}$$

Apparently, the expression above shows that the beampattern formed by FDA is related not only to the angle, but also to the range and the time, which is greatly different from the traditional PA with only angle-dependent beampattern.

Apart from the above linear frequency offset, several other types of frequency offset, such as logarithmic and random frequency offset, are also studied in existing works [28]–[30]. Compared with the standard FDA, whose beampattern is a continuous and homogeneous S-like curve, these new types of FDA break the regular beampattern into several clusters in the range-angle map.

Inspired by these nonlinear FDAs, we proposed a novel finite orthogonal random (FOR) FDA, which can generate a

series of pulsed beampattern in specified directions without any implement of the pulse generator (see Fig. 2). The frequency offsets of FOR-FDA are randomly selected from a finite set of an integer multiple of a basic frequency offset f_d, which can be expressed as

$$\mathcal{S}_L = \{f_d, 2f_d, \cdots, Lf_d\}, \tag{5}$$

where $L \leq N$ denotes the number of elements in the frequency set.

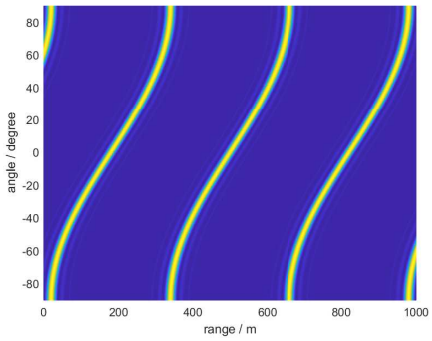

(a) Beampattern of standard FDA.

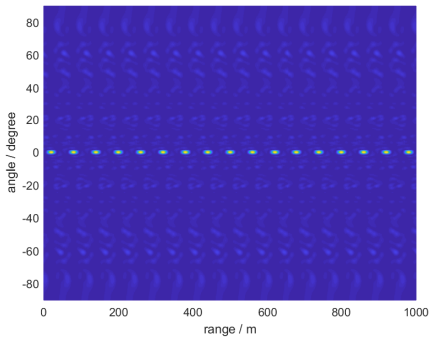

(b) Beampattern of FOR-FDA.

Fig. 2: Demonstrations of different FDA beampatterns.

The beampattern of the FOR-FDA features a series of homogeneous pulses in the time or range domain. By taking advantage of this beampattern, one can either measure the distance of targets by the received pulse delay, or jointly estimate its angle and distance by the signal processing method [31], which can provide a more accurate localization compared with the conventional PA Radar. However, since the localization algorithms are beyond the scope of this article, we will address it in our future works.

III. Dual-functional RadComm System Model

In this section, we propose the scheme of the joint PA and FDA dual-functional system and establish the model of RadComm system.

A. Joint PA and FDA Scheme

We design the scheme of joint PA and FDA dual-functional system as depicted in Fig. 3. In this system, an N-element ULA antenna is fully shared by PA and FDA. Communications data $\mathbf{s}(t)$ and Radar signal of continuous sinusoidal wave $s_0(t)$ are emitted through the N-element antenna array, simultaneously. We assume $\mathbb{E}[\mathbf{s}(t)\mathbf{s}^H(t)] = \mathbf{I}$ and $\mathbb{E}[s_0(t)s_0^*(t)] = 1$, where $(\cdot)^H$ is the Hermitian operation, $(\cdot)^*$ is the conjugate operation, and $\mathbb{E}$ denotes the mathematical expectation.

We first consider the part of the communications with PA. Assume the l-th sample vector of the N data streams $\mathbf{s}(l) = [s_1(l)\ s_2(l)\ \cdots\ s_N(l)]^T$ is input into the digital precoding matrix $\mathbf{W}$, then passed through the N RF chains, and finally radiated into the wireless channel by the N antenna elements.

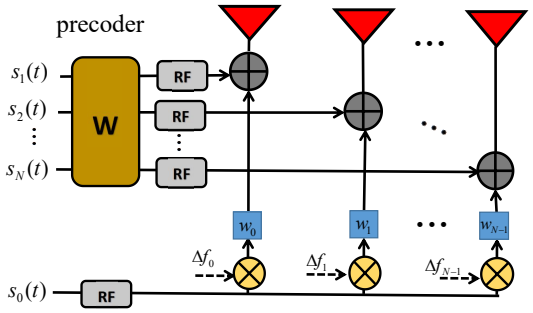

Fig. 3: Joint PA and FDA dual-functional system.

As for the part of the Radar with FDA, the l-th sample of the Radar signal $s_0(l)$ first goes through its RF chain and then is divided into N ways by a divider. In each way, a specific frequency offset Δf_n randomly selected from the frequency set $\mathcal{S}_L$ is added to the RF signal by its corresponding mixer. With the weights assigned by the phase shifters and amplifiers, all the processed Radar signals are finally radiated by the corresponding antenna elements.

The benefits of this structure, on the one hand, can save the equipment of hardware such as antennas, which can make the system more compact. In addition, the RadComm system can easily share the common information and parameters, i.e., DOA and channel state information (CSI), which significantly reduces the computational resource for both Radar and communications.

B. System Model

The system model of RadComm is illustrated in Fig. 4. In this system, the joint PA and FDA RadComm transmitter with N-element array communicates with the mobile station (MS), which is equipped with an M-element PA antena, and detects targets through the FDA antenna, simultaneously.

For the Radar part, Radar signals are emitted by the Radar transmitter (RadTx) and reflected by targets to another Radar receiver (RadRx). For simplicity, we assume the RadRx is equipped with a single directional antenna.

For the communications part, we assume the channel between the communications transmitter (CommTx) and the MS as the geometric MIMO channel model [33]–[37] with K clusters. In this work, we only consider the downlink communications.

1) Channel model: We center the transmitter and assume K clusters are located at $\{(\theta_k, r_k), k = 1, 2, \cdots, K\}$, where

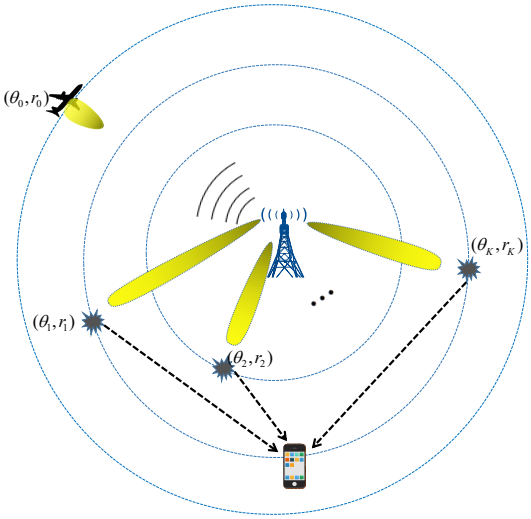

Fig. 4: System Model

θ_k and r_k are the angle and range of the kth cluster, while the target is located at (θ_0, r_0), where θ_0 and r_0 is the angle and range of the target.

We first consider the interference channel from the RadTx to the MS. The electromagnetic wave rays with L frequencies transmitted from the N-element RadTx are reflected to the M-element MS by K clusters. It should be noted is that each antenna at the MS can receive all the L-frequencies waves from every cluster. Under this physical model, we build the channel model from the FDA RadTx to the PA MS as

$$\mathbf{H}_{\text{PF}} = \sum_{k=1}^{K} \alpha_k \Big(\sum_{l=1}^{L} \mathbf{a}_{\text{PA}}(\phi_k, \lambda_l) \Big) \mathbf{a}_{\text{FDA}}^H(\theta_k, r_k, t) \tag{6}$$

where ϕ_k denotes the angle of the kth cluster with respect to the MS, λ_l is the wavelength of the l-th carrier frequency at the RadTx side, α_k is the complex gain of the kth path, and $\mathbf{a}_{\text{PA}}(\phi_k, \lambda_l)$ as well as $\mathbf{a}_{\text{FDA}}(\theta_k, r_k, t)$ are the antenna array steering vectors of PA and FDA, respectively.

If ULA is employed, $\mathbf{a}_{\text{FDA}}(\theta, r, t)$ can be written as

$$\mathbf{a}_{\text{FDA}}(\theta, r, t) = \frac{1}{\sqrt{N}} [e^{j2\pi\psi_0}, e^{j2\pi\psi_1}, \cdots, e^{j2\pi\psi_{N-1}}]^T, \tag{7}$$

where $\psi_n = n\frac{d}{\lambda_0}\sin\theta - \frac{\Delta f_n}{c_0} r + \Delta f_n t$, and d is the distance between any neighbour antenna elements.

The PA steering vector $\mathbf{a}_{\text{PA}}(\phi, \lambda)$ can be formulated as

$$\mathbf{a}_{\text{PA}}(\phi, \lambda) = \frac{1}{\sqrt{MN}} [1, e^{j\frac{2\pi}{\lambda} d\sin\phi}, \cdots, e^{j(M-1)\frac{2\pi}{\lambda} d\sin\phi}]^T. \tag{8}$$

For simplicity, the channel can be written into a more compact form

$$\mathbf{H}_{\text{PF}} = \mathbf{A}_{\text{PA}} \mathbf{\Lambda} \mathbf{A}_{\text{FDA}}^H, \tag{9}$$

where

$$\mathbf{\Lambda} = \text{diag}\{\alpha_1, \alpha_2, \cdots, \alpha_K\}, \tag{10}$$

$$\mathbf{A}_{\text{FDA}} = [\mathbf{a}_{\text{FDA}}(\theta_1, r_1, t), \ \cdots, \mathbf{a}_{\text{FDA}}(\theta_K, r_K, t)], \tag{11}$$

$$\mathbf{A}_{\text{PA}} = \sum_{l=1}^{L} [\mathbf{a}_{\text{PA}}(\phi_1, \lambda_l), \ \cdots, \ \mathbf{a}_{\text{PA}}(\phi_K, \lambda_l)]. \tag{12}$$

Then, we study the channel from the CommTx to the MS. Assuming the wavelength of the carrier frequency of communications signals is λ_C, which is approximated to the wavelength of Radar signals, then the path loss $\mathbf{\Lambda}$ can be considered as the same as $\mathbf{H}_{\text{PF}}$. Hence, the channel from the CommTx to the MS can be expressed by

$$\begin{aligned} \mathbf{H}_{\text{PP}} &= \sum_{k=1}^{K} \alpha_k \mathbf{b}_{\text{MS}}(\phi_k) \mathbf{b}_{\text{BS}}^H(\theta_k) \\ &= \mathbf{B}_{\text{MS}} \mathbf{\Lambda} \mathbf{B}_{\text{BS}}^H \end{aligned} \tag{13}$$

where

$$\mathbf{b}_{\text{MS}}(\phi_k) = \frac{1}{\sqrt{M}} [1, e^{j\frac{2\pi}{\lambda_C} d\sin\phi_k}, \cdots, e^{j(M-1)\frac{2\pi}{\lambda_C} d\sin\phi_k}]^T, \tag{14}$$

$$\mathbf{b}_{\text{BS}}(\theta_k) = \frac{1}{\sqrt{N}} [1, e^{j\frac{2\pi}{\lambda_C} d\sin\theta_k}, \cdots, e^{j(N-1)\frac{2\pi}{\lambda_C} d\sin\theta_k}]^T, \tag{15}$$

$$\mathbf{B}_{\text{MS}} = [\mathbf{b}_{\text{MS}}(\phi_1), \ \mathbf{b}_{\text{MS}}(\phi_2), \cdots, \mathbf{b}_{\text{MS}}(\phi_K)], \tag{16}$$

$$\mathbf{B}_{\text{BS}} = [\mathbf{b}_{\text{BS}}(\theta_1), \ \mathbf{b}_{\text{BS}}(\theta_2), \cdots, \mathbf{b}_{\text{BS}}(\theta_K)]. \tag{17}$$

2) Radar Detection: As mentioned previously, compared with the conventional PA Radar, the FDA Radar employs different frequencies for each element. Hence, the bandwidths of the FDA can be way wider than that of the PA Radar and communications system. Besides, the discrete FDA pulsed beampatterns also reduce the overlapped time with communications. We denote the overlapped rate of bandwidths and time of the FDA Radar and communications by μ. Then the l-th sample of received signal at the RadRx can be written by

$$\begin{aligned} y_R(l) =& \alpha_0 \sqrt{pP_0} \mathbf{a}_{\text{FDA}}^H(\theta_0, r_0, t) \mathbf{w} s_0(l) \\ &+ \beta_0 \mu \sqrt{(1-p)P_0} \mathbf{b}_{\text{BS}}^H(\theta_R) \mathbf{W} \mathbf{s}(l) + n_R(l), \end{aligned} \tag{18}$$

where $\mathbf{w} \in \mathbb{C}^N$ with $||\mathbf{w}|| = 1$ is the weights of the Radar signal, $\mathbf{W} \in \mathbb{C}^{N\times N}$ with $||\mathbf{W}|| = 1$ is the digital precoder of the communications signals, α_0 is the path gain from the RadTx to the RadRx through the target, β_0 is the path gain from the CommTx directly to the RadRx, P_0 is the total system power and $p \in [0, 1]$ denotes the power split ratio of the Radar power over the total power, θ_R denotes the angle of the RadRx with respect to RadTx, and $n_R(l) \sim \mathcal{CN}(0, \sigma_R^2)$ is the additive Gaussian white noise (AWGN) with zero-mean and variance σ_R^2.

Since $\mathbb{E}[\mathbf{s}(l)\mathbf{s}^H(l)] = \mathbf{I}$ and $\mathbb{E}[s_0(l)s_0^*(l)] = 1$, the SINR at the received Radar can be expressed as

$$\text{SINR}_{\text{T}} = \frac{pP_0|\alpha_0|^2 \mathbf{w}^H \mathbf{a}_{\text{FDA}}(\theta_0, r_0) \mathbf{a}_{\text{FDA}}^H(\theta_0, r_0) \mathbf{w}}{(1-p)P_0|\mu\beta_0|^2 \mathbf{b}_{\text{BS}}^H(\theta_R) \mathbf{W}\mathbf{W}^H \mathbf{b}_{\text{BS}}(\theta_R) + \sigma_R^2}. \tag{19}$$

3) Communications: The main task of the communications part is that the CommTx has to transmitted its signals to the MS with high SINR. According to the channel model in this section, the received signal at the MS can be formulated as

$$\mathbf{y}_{\text{MS}}(l) = \sqrt{(1-p)P_0}\mathbf{H}_{\text{PP}}\mathbf{W}\mathbf{s}(l)+\sqrt{pP_0}\mu\mathbf{H}_{\text{PF}}\mathbf{w}s_0(l)+\mathbf{n}_M(l), \tag{20}$$

where $\mathbf{n}_M$ is the vector of independent and identically distributed (i.i.d) AWGN of $\mathcal{CN}(\mathbf{0}, \sigma_M^2\mathbf{I}_M)$, where the $\mathbf{I}_M$ is the identity matrix.

Hence, the SINR at the MS can be expressed as

$$\text{SINR}_{\text{MS}} = \frac{(1-p)P_0 tr(\mathbf{H}_{\text{PP}}\mathbf{W}\mathbf{W}^H\mathbf{H}_{\text{PP}}^H)}{pP_0\mu^2\mathbf{w}^H\mathbf{H}_{\text{PF}}^H\mathbf{H}_{\text{PF}}\mathbf{w}+\sigma_M^2}. \tag{21}$$

Then, the maximum achieved rate between the MS and BS assuming Gaussian signaling is

$$R_P = \log_2(1+\frac{(1-p)P_0 tr(\mathbf{H}_{\text{PP}}\mathbf{W}\mathbf{W}^H\mathbf{H}_{\text{PP}}^H)}{pP_0\mu^2\mathbf{w}^H\mathbf{H}_{\text{PF}}^H\mathbf{H}_{\text{PF}}\mathbf{w}+\sigma_M^2}). \tag{22}$$

IV. Joint PA and FDA beamforming

In the RadComm system, our task, on the one hand, is to guarantee the high detection probability of the target, on the other hand, is to maximize the quality of the communications between the MS and BS. In other words, we can formulate this problem as a multiple objectives optimization: maximizing the SINRs of the received signals for both Radar and communications, which can be expressed by

$$\begin{aligned} \max_{\mathbf{w},\mathbf{W}} \quad & \text{SINR}_{\text{T}},\ \text{SINR}_{\text{MS}} \\ s.t. \quad & ||\mathbf{w}|| = 1, \\ & ||\mathbf{W}|| = 1. \end{aligned} \tag{23}$$

A. Ratio-Maximizing Approach

In fact, to maximize the SINRs of Radar and communications, it needs to enhance the power to the directions of target and MS (or the clusters) by the RadTx and CommTx respectively and reduce its power to the interference directions.

Hence, an intuitive strategy to tackle this problem is breaking the problem of (23) into the following two sub-problems:

$$\begin{aligned} \max_{\mathbf{w}} \quad & \frac{\mathbf{w}^H\mathbf{A}(\theta_0, r_0)\mathbf{w}}{\mathbf{w}^H\mathbf{H}_{\text{PF}}^H\mathbf{H}_{\text{PF}}\mathbf{w}} \\ s.t. \quad & ||\mathbf{w}|| = 1, \end{aligned} \tag{24a}$$

$$\begin{aligned} \max_{\mathbf{W}} \quad & \frac{tr(\mathbf{H}_{\text{PP}}\mathbf{W}\mathbf{W}^H\mathbf{H}_{\text{PP}}^H)}{\mathbf{b}_{\text{BS}}^H(\theta_R)\mathbf{W}\mathbf{W}^H\mathbf{b}_{\text{BS}}(\theta_R)} \\ s.t. \quad & ||\mathbf{W}|| = 1, \end{aligned} \tag{24b}$$

where $\mathbf{A}(\theta_0, r_0) = \int_\Omega \mathbf{a}_{\text{FDA}}(\theta, r, t)\mathbf{a}_{\text{FDA}}^H(\theta, r, t)d\theta$, in which the Ω is the angle domain of FDA beampattern towards the target, which can be expressed as

$$\Omega \triangleq \{\theta | \theta_0 - \nu \le \theta \le \theta_0 + \nu\}, \tag{25}$$

where ν denotes the half beampattern width in angle domain.

Then the (n, m)-th element in $\mathbf{A}(\theta_0, r_0)$ can be expressed as (26) at the top of next page.

Proposition 1: *If* $\mathbf{A}$ *is positive-definite and Hermitian matrix, the optimization problem of (32) can be recast to find the eigenvector corresponding to the largest generalized eigenvalues as follows*

$$\mathbf{w}^{opt} : \mathbf{A}\mathbf{w}^{opt} = \lambda_{max}\mathbf{H}_{PF}^H\mathbf{H}_{PF}\mathbf{w}^{opt} \tag{27}$$

where λ_{max} *and* $\mathbf{w}_F^{opt}$ *denote the maximum generalized eigenvalue and the corresponding generalized eigenvector, respectively.* □

According to Proposition 1, the optimal beamformer for the FDA Radar can be directly obtained.

Now, we are at a position to discuss the second sub-problem of (24b). For simplicity, we define the objective function as

$$h(\mathbf{W}) = \frac{tr(\mathbf{H}_{\text{PP}}\mathbf{W}\mathbf{W}^H\mathbf{H}_{\text{PP}}^H)}{\mathbf{b}_{\text{BS}}^H(\theta_R)\mathbf{W}\mathbf{W}^H\mathbf{b}_{\text{BS}}(\theta_R)}. \tag{28}$$

We first deduce the gradient of $h(\mathbf{W})$ with respect to $\mathbf{W}$, then employ the steepest descent method to update $\mathbf{W}$ and normalize it at each iteration to meet the power constraint.

With several straightforward derivations, the gradient of $h(\mathbf{W})$ with respect to $\mathbf{W}$ can be expressed as

$$\begin{aligned} \nabla h(\mathbf{W}) = \frac{2}{||\mathbf{W}^H\mathbf{b}_{\text{BS}}||^4}(&\mathbf{H}_{\text{PP}}^H\mathbf{H}_{\text{PP}}\mathbf{W}\mathbf{b}_{\text{BS}}^H(\theta_R)\mathbf{W}\mathbf{W}^H\mathbf{b}_{\text{BS}} \\ &- tr(\mathbf{H}_{\text{PP}}\mathbf{W}\mathbf{W}^H\mathbf{H}_{\text{PP}}^H)\mathbf{b}_{\text{BS}}\mathbf{b}_{\text{BS}}^H\mathbf{W}). \end{aligned} \tag{29}$$

According to the steepest descent method, we update $\mathbf{W}$ by

$$\mathbf{W}_{k+1} = \mathbf{W}_k + \delta\nabla h(\mathbf{W}_k). \tag{30}$$

where $\mathbf{W}_k$ denotes the precoding matrix at the k-th iteration.

To meet the power constraint, we normalize $\mathbf{W}$ by

$$\mathbf{W}_{k+1} = \mathbf{W}_{k+1}/||\mathbf{W}_{k+1}||. \tag{31}$$

In additions, to increase the convergence rate, we employ the Armijo rule of the backtracking line search [32] to determine the step size of each iteration. The precoding algorithm of the communications can be summarized as Algorithm 1, where δ denotes step size, ε is small threshold, $\xi \in (0, 0.5)$ and $\kappa \in (0, 1)$.

Algorithm 1 Algorithm for the precoder of communications.

```
Initialize δ = δ_max;
while ||∇h(W_k)|| > ε do
    while h(W_k + δ ∇h(W_k)/||∇h(W_k)||) > h(W_k) − ξδ||∇h(W_k)|| do
        δ ⇐ κδ;
    end while
    W_{k+1} = W_k + δ ∇h(W_k)/||∇h(W_k)||;
    x_{k+1} = x_{k+1}/||W_{k+1}||;
end while
```

However, since the denominators in (24) are small when the number of antenna elements is large, the solution of (24) becomes unstable. In fact, the obtained solutions from (24a) and (24b) tend to find small denominators rathere than large numerators due to huge difference in profit weights:

$$
\begin{aligned}
A_{n,m} &= \int_{\Omega} \exp\{j2\pi(nf_0 d\sin\theta/c_0 - \Delta f_n r/c_0 + \Delta f_n t)\}\exp\{-j2\pi(mf_0 d\sin\theta/c_0 - \Delta f_m r/c_0 + \Delta f_m t)\}d\theta \\
&= \int_{\theta_0-\nu}^{\theta_0+\nu} \exp\{j2\pi(n-m)d\sin\theta/\lambda_0\}d\theta \exp\{j2\pi(\Delta f_m - \Delta f_n)r/c_0\}\exp\{j2\pi(\Delta f_n - \Delta f_m)t\} \\
&\approx \exp\{j2\pi(n-m)d\sin\theta_0/\lambda_0\}\frac{\cos[2\pi(n-m)d\cos\theta_0\nu/\lambda_0]}{j\pi(n-m)d\cos\theta_0\nu/\lambda_0}\exp\{j2\pi(\Delta f_m - \Delta f_n)r/c_0\}\exp\{j2\pi(\Delta f_n - \Delta f_m)t\}
\end{aligned} \tag{26}
$$

a small change for denominators can get huge profit, while for numerators can get nearly nothing. In other words, the unstable solutions of the optimization (24) pay more attention to minimizing the signal interference rather than maximizing the power of received signals.

B. QCQP Approach

When considering the small interference of the RadComm, there is an alternative way to solve the problem (23), which can be expressed as

$$
\begin{aligned}
\max_{\mathbf{w}} \quad & \mathbf{w}^H\mathbf{A}(\theta_0, r_0)\mathbf{w} \\
s.t. \quad & \mathbf{w}^H\mathbf{H}_{\text{PF}}^H\mathbf{H}_{\text{PF}}\mathbf{w} \le I_R \\
& ||\mathbf{w}|| = 1,
\end{aligned} \tag{32a}
$$

$$
\begin{aligned}
\max_{\mathbf{W}} \quad & tr(\mathbf{H}_{\text{PP}}\mathbf{W}\mathbf{W}^H\mathbf{H}_{\text{PP}}^H) \\
s.t. \quad & \mathbf{b}_{\text{BS}}^H(\theta_R)\mathbf{W}\mathbf{W}^H\mathbf{b}_{\text{BS}}(\theta_R) \le I_M \\
& ||\mathbf{W}|| = 1.
\end{aligned} \tag{32b}
$$

where I_R, I_M are pre-values of the thresholds of interference powers for Radar and communications, respectively.

In fact, both (32a) and (32b) are belong to quadratically constrained quadratic programming (QCQP) problem, which is not convex. Nevertheless, an approximate solution of this problem can be obtained by a semi-definite relaxation approach [39]. According to the relaxation steps in [39], the beamfomer of $\mathbf{w}$ and $\mathbf{W}$ can be obtained through interior-point algorithms. To ensure the satisfaction of power constraints, we normalize the obtained approximate beamformers at each iteration.

C. Complexity Analysis

Assume that the arithmetic with individual elements has a complexity of $\mathcal{O}(1)$, and we ignore the operations of addition and subtraction. The computational complexity of multiplying an $n \times m$ matrix by an $m \times p$ matrix is $\mathcal{O}(nmp)$. The computational complexity of the SVD for an $m \times n$ matrix ($m \le n$) is $\mathcal{O}(mn^2)$. The computational complexity of the $n \times n$ matrix inversion is $\mathcal{O}(n^3)$ (assume we adopt the GaussJordan elimination method). Then, for each iteration, the complexity of the Ratio-Maximizing and the QCQP algorithms are same as to $\mathcal{O}(N^3)$.

V. Channel Estimation Imprecision

The proposed beamforming algorithms are based on the perfect knowledge of CSI. However, the perfect estimation of channel from the Radar to the MS is not easy to obtain in practice due to the absence of transmission of pilot signals. In this section, we focus on scenarios in which this perfect knowledge can not be got, and the uncertain channel model is built by a known probability distribution. We extend the previous beamforming algorithms to account for such uncertain channel model and make sure that the probability that the interference power is above I_R remains below a given value.

Since the channel related to FDA signals consists of different frequency offsets, and different estimation errors have to be obtained corresponding to these different frequencies. Similar to [38], we consider the real channel $\mathbf{H}_{\text{PF}}$ is related to its estimate $\hat{\mathbf{H}}_{\text{PF}}$ through the following expression

$$
\mathbf{H}_{\text{PF}}[f] = \hat{\mathbf{H}}_{\text{PF}}[f] + \mathbf{H}_{\text{PF}}^e[f], \tag{33}
$$

where $f \in \{1, 2, \cdots, L\}$ denotes the index of frequency, $\mathbf{H}_{\text{PF}}^e$ is the channel estimation error that follows a known priori probability distribution. More particularly knowledge of the distribution of the squared norm of this error, defined by

$$
e(f) = ||\mathbf{H}_{\text{PF}}^e[f]||^2, \tag{34}
$$

can be robustified beamformer designs. To this end, we assume that the RadTx aims at selecting a beamformer such as to ensure that the interference constraint can be met with a given probability $\mathcal{P}$, which can be expressed as

$$
Pr\Big(\sum_{f=1}^{M} ||(\hat{\mathbf{H}}_{\text{PF}}[f] + \mathbf{H}_{\text{PF}}^e[f])\mathbf{w}||^2 \le I_R\Big) \ge \mathcal{P}. \tag{35}
$$

Now, we give a theorem that can satisfy this constrain with the knowledge of the cumulative distribution function (CDF) $\mathcal{F}_e(\cdot)$ of $\sum_{f=1}^{M} e(f)$.

Theorem 1: A feasible solution satifying the (35) can be obtained by solving the following optimization problem

$$
\begin{aligned}
\max_{\mathbf{w}} \quad & ||\mathbf{w}^H\mathbf{A}(\theta_0, r_0)\mathbf{w}||^2 \\
s.t. \quad & ||\hat{\mathbf{H}}_{\text{PF}}\mathbf{w}||^2 \le \Big(\sqrt{i_R} - \sqrt{\frac{\mathcal{F}^{-1}(\mathcal{P})}{M}}\Big)^2, \\
& ||\mathbf{w}|| = 1.
\end{aligned} \tag{36}
$$

where $i_R = I_R/M$.

Proof: We notice that $||\mathbf{H}_{\text{PF}}^e\mathbf{w}||^2 \le e(f)$, and according to the Cauchy-Schwarz inequality, we can rewrite the interference constraint in (32a) as in (37) at the top of next page.

For the simplicity, we define

$$\sum_{f=1}^{M}||(\hat{\mathbf{H}}_{\text{PF}}[f]+\mathbf{H}_{\text{PF}}^{e}[f])\mathbf{w}||^2 \le \sum_{f=1}^{M}||\hat{\mathbf{H}}_{\text{PF}}[f]\mathbf{w}||^2+\sum_{f=1}^{M}e(f)+2\sqrt{\sum_{f=1}^{M}||\hat{\mathbf{H}}_{\text{PF}}[f]\mathbf{w}||^2\cdot\sum_{f=1}^{M}e(f)} \le I_R \tag{37}$$

$$\mathcal{A} \triangleq \left(\sqrt{I_R}-\sqrt{\sum_{f=1}^{M}||\hat{\mathbf{H}}_{\text{PF}}[f]\mathbf{w}||^2}\right)^2. \tag{38}$$

Then, with several simply derivations, it can be shown that the inequality (37) can be hold provided that

$$0 \le \sum_{f=1}^{M} e(f) \le \mathcal{A}. \tag{39}$$

Inequality (39) is valid provided that $\sqrt{I_R} \ge \sqrt{\sum_{f=1}^{M}||\hat{\mathbf{H}}_{\text{PF}}[f]\mathbf{w}||^2}$, and we can ensure that the probabilistic constraint is satisfied given

$$\mathcal{F}_e(\mathcal{A}) \ge \mathcal{P}, \tag{40}$$

which is equivalent to

$$\frac{1}{M}\sum_{f=1}^{M}||\hat{\mathbf{H}}_{\text{PF}}[f]\mathbf{w}||^2 \le \left(\sqrt{i_R}-\sqrt{\frac{\mathcal{F}^{-1}(\mathcal{P})}{M}}\right)^2 \tag{41}$$

A more restrictive condition can be converted as follow:

$$||\hat{\mathbf{H}}_{\text{PF}}\mathbf{w}||^2 \le \left(\sqrt{i_R}-\sqrt{\frac{\mathcal{F}^{-1}(\mathcal{P})}{M}}\right)^2 \tag{42}$$

That completes the proof.

□

Theorem 1 shows that the robust case consists of an extra constant and does not increase any computational complexity of the optimization problem.

VI. Numerical Analysis

In this section, numerical results are provided to demonstrate the performance of the proposed joint PA and FDA beamforming by comparing with the traditional PA beamforming. Unless otherwise explicitly stated, we use the following default values for the system parameters. The transmitter is equipped with a ULA of $N = 32$ antennas. For the communications part, we consider the MS is equipped with a ULA of $M = 4$ receiving antennas. While for the Radar part, the main carrier frequency is set to $f_0 = 10$ GHz, the basic frequency offset $f_d = 5$ MHz, the number of elements in the frequency set $L = 5$ and the distance between antenna elements is $d = c_0/2f_0$. Besides, we assume that signals are transferred from the BS to the MS located at $(\theta_0, r_0) = (0°, 500m)$ through $K = 5$ clusters. Assume the locations of the five clusters is at $C_1(-70°, 197m)$, $C_2(-45°, 610m)$, $C_3(20°, 651m)$, $C_4(60°, 287m)$, $C_5(70°, 732m)$, and the angle of the RadRx is $\theta_R = -10°$. Others parameters are summarized in the following Table I.

TABLE I: Parameters list.

parameters	ν	$\delta_{\max}$	ε	ξ	κ	μ
vaules	0.01	1	10^{-3}	0.5	0.9	0.1

A. Beam Patterns with Different Frequency Offsets

To study the impacts of the configurations of frequency offsets to beampatterns, we presented four types of frequency offsets. The first one is that all the frequency offsets are zeros, which in fact is the conventional PA. The second one is the standard FDA with linearly increasing frequency offsets along with antenna elements, i.e., $\Delta f_n = nf_d$ for the nth element. The third one is the Log-FDA with logarithmically increasing frequency offsets:

$$\Delta f_n = \log(n+1)f_d. \tag{43}$$

The last one is the proposed FOR-FDA. In this simulation, each frequency offset is randomly selected from $\mathcal{S}_5 = \{f_d, 2f_d, \cdots, 5f_d\}$.

Fig. 5(a)-(d) shows the beampatterns of the above four different frequency offsets in the angle-range domain, respectively. Fig. 5a depicts the beampattern of the conventional PA, which can be considered as a special FDA with none frequency offsets. It is a straight ray in the angle-range map, so it is only insensitive to the angle domain but not to the range (or time) domain. The beampattern of the standard FDA in Fig. 5b significantly varies with respect to both angle and range. Besides, its peak region is a continued narrow S-like belt in the angle-range domain. Hence, the beampatterns of the standard FDA cannot focus their powers to a target located at a certain angle. The beampatterns of the Log-FDA and proposed FOR-FDA in Fig. 5c and Fig. 5d have the ability to break the continued beampattern into pieces. Nevertheless, compared with the FOR-FDA, the beampattern of the Log-FDA has two very large blurry 'tails' on both sides of its main body, which may lead to a low resolution in the angle and range (or time) domains. In contrast, the proposed FDA can generate a sequential periodical short pulses with multiple orthogonal frequencies. With such a beampattern, the Radar can accurately estimate the target at both angle and range domains simultaneously [31].

B. Multi-objective Optimization

Now, we evaluate the performance of the SINR_{T} and SINR_{MS} with respect to different power split ratio p and total power P_0. In this simulation, we assume the received noise variances of the MS and RadRx are both equal to 0.1.

To compare the performances of different algorithms and schemes, we separately simulate the performances of the conventional PA method, the joint PA and FDA with different solutions of (24) and (32), and the joint PA and FDA with

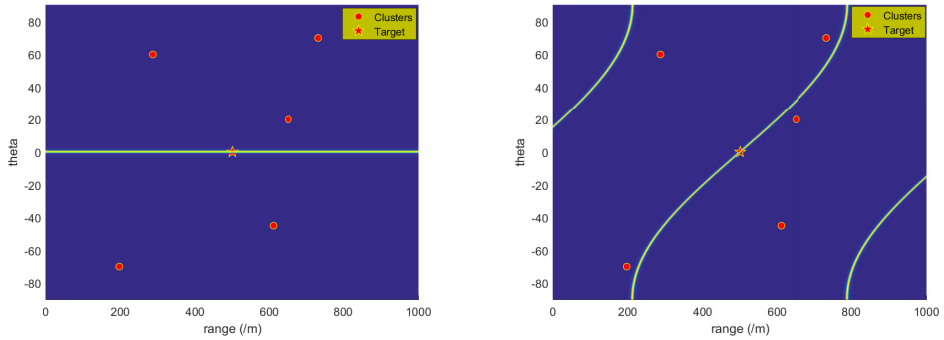

(a) Conventional PA. (b) Standard FDA.

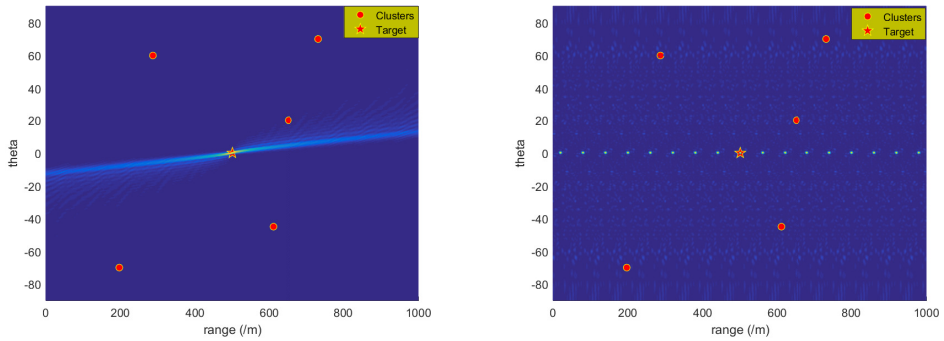

(c) Log-FDA. (d) Proposed FOR-FDA.

Fig. 5: Comparison of beampatterns for different freqnency offsets.

separated deployment using the algorithm of (32), where half antenna elements are used for the communications and the rest are used for the Radar. In this simulation, the total power P_0 is set to 100, and the power split ratio ranges from 0 to 1 with the step of 0.1.

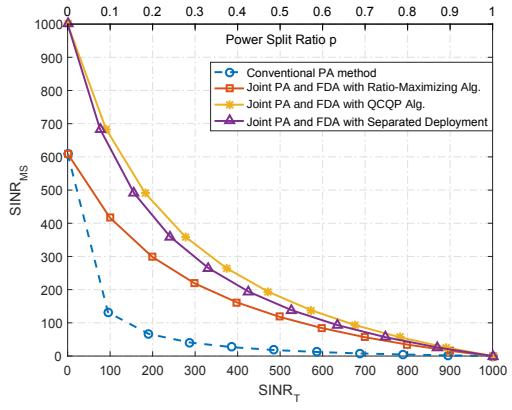

Fig. 6: Joint optimization with $M = 16, P_0 = 100$.

Fig. 6 depicts that the performances of different methods with 16 antennas. The simulations results show that the joint SINR_T and SINR_MS of the proposed FOR-FDA is distinctly better than that of the conventional PA. This is because, on the one hand, that the frequency bandwidths of FDA can be much broader than that of PA, and on the other hand, the overlapped resource rate of Radar FDA signals and communication data is fewer than that of the conventional PA scheme. Due to the solution of Ratio-Maximizing algorithm is unstable, the average performances is a little lower than that of the QCQP algorithm. For the separated deployment, due to its few degrees of freedom (DoF) for both communications and Radar, the performance is not superior to the shared deployment scheme, although the separated one may generate less interference power budget.

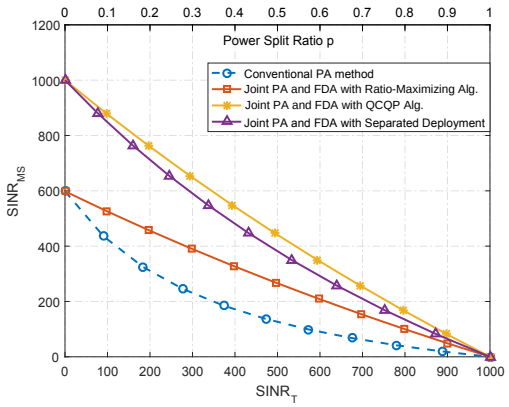

Fig. 7: Joint optimization with $M = 32, P_0 = 100$.

Fig. 7 demonstrates the joint communications and Radar optimization with antenna number of 32, while other parameters maintain the same as the previous simulation. Compared with Fig. 6, the curves in Fig. 7 tend to straight lines, which means that with the same power split ratio, Fig. 7 can get higher SINRs for both communications and Radar simultaneously

than that of Fig. 6. In other words, with more antennas, the RadComm system can harvest more array gains and hence get extra SINRs gains.

C. Impacts of Antenna Numbers

To study the impacts of the antenna numbers to the performance of our proposed method, we jointly optimize the SINR of the communications and Radar by the proposed QCQP approach with antenna numbers varying from 16 to 128.

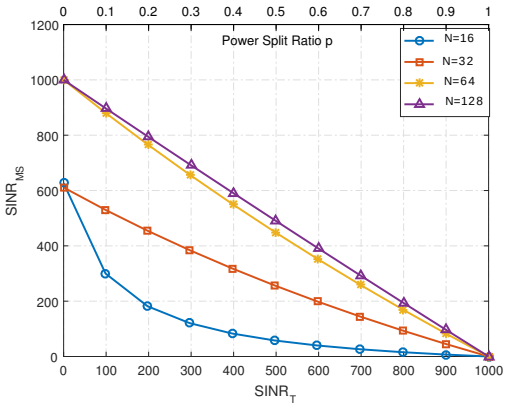

Fig. 8: Joint optimization with different number of transmitting antennas.

Fig. 8 shows that as the number of antenna elements increases, the curves performances of tend to straight line, which is consistent with the previous simulations. However, when the number of the antennas exceeds 64, the performance gain becomes insignificant, even though the antenna number dramatically increases. This is because when the antenna number arrives at a particular value, the performance of RadComm is mainly determined by the total system power. To demonstrate this point, we did another simulation with different values of total power in Subsection D.

D. Impacts of Total System Power

In this subsection, to examine the impacts of the total system power to the joint optimization problem, we simulated the proposed algorithm of (32) when the total power varies from 50 to 200 with step size of 50. The antenna number is set to 32.

It should be noted that there are 11 marks on each curve in Fig. 9, and the k-th mark is generated by the power split ratio of $p = k/10$. Fig. 9 implies that as the total power increase, the performance of joint optimization of communications and Radar is significantly improved. When the SINR_{MS} is maintained at a certain level, the SINR_{T} almost linearly increases along with the changes of total power.

E. FOR-FDA pulse Parameters

Now, let us examine the pulse parameters. Fig. 10 and Fig. 11 depict the FOR-FDA pulse in angle and range domains. In this subsection, we want to examine what factors determine the shape of the FOR-FDA pulses.

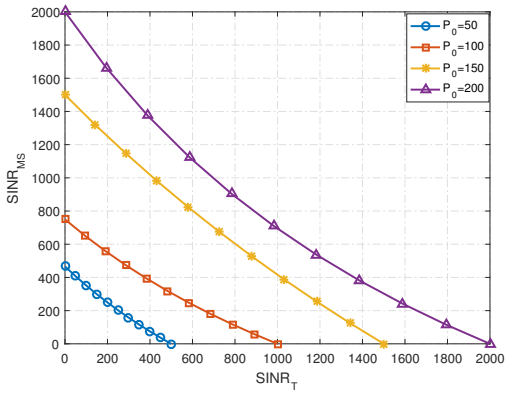

Fig. 9: Joint optimization with different total powers.

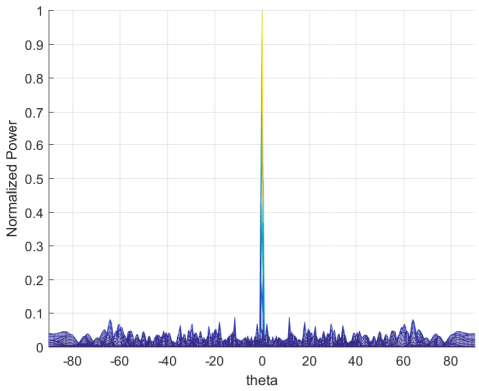

Fig. 10: FOR-FDA pulse in angle domain.

Since the frequency offset is randomly selected from a given integral set, it is not easy to express the analytical formulation of the synthesized beampatterns. However, the periodical frequency offset can help us to understand the mechanism of the FOR-FDA pulse. The difference between the beampatterns of periodically and randomly selected frequency offset is that except their same main lobes, there are two more grating lobes in the beampattern generated by the periodical frequency offset.

For simplicity, we consider a bi-frequency periodical frequency offsets, given as follows

$$\Delta f_n = \frac{1+(-1)^n}{2} f_d. \tag{44}$$

Assume the antenna number N is odd, and all other parameters are the same as those in Section II except the frequency offset Δf_n, then we can deduce the expression of the beampattern power as follows (Appendix A)

$$P = \left| 2\cos(\pi \Delta f (t - r/c_0) - \pi d \sin\theta/\lambda_0) \frac{\sin(N-1)\pi d \sin\theta/2\lambda_0}{\sin 2\pi d \sin\theta/\lambda_0} \right|^2. \tag{45}$$

The beampatterns in angle-range map is shown in Fig. 12.

From (45) and Fig. 12 we can see although there are two big grating lobes when $\theta = \pm 90^\circ$, the beampattern still maintains the lobe at $\theta = 0^\circ$. (45) shows that the pulse width in time or range domain is related to Δf, and the pulse width in angle domain is determined by N.

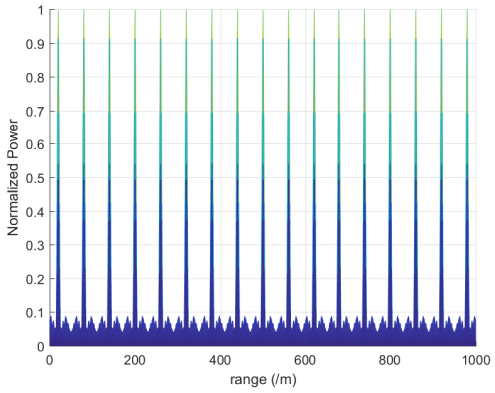

Fig. 11: FOR-FDA pulse in range (or time) domain.

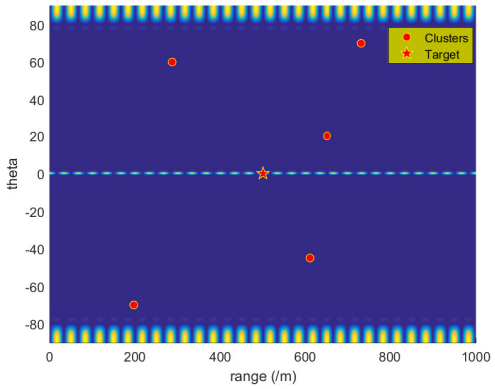

Fig. 12: Beampatterns of the FDA with bi-frequency periodical frequency offsets.

When further deduce the expressions of the beampatterns for tri-frequency and other multi-frequency, we find that the pulse width and period in time or range domain is determined by $(L-1)f_d$, where L denotes the number of elements in the frequency set $\mathcal{S}_L$. In fact, it is also the result of the uncertainty principle, which means the product of time and bandwidth is not smaller than a given constant. The shorter the pulse in time domain is, the wider it occupies frequency bandwidth. Besides, the pulse power is determined by the number of antenna elements and the transmitted power.

F. Convergence Analysis

Let us now study the convergence rate for the Ratio-Maximizing and QCQP approaches.

Fig. 13 and Fig. 14 show that convergence rates for the Ratio-Maximizing and the QCQP algorithms using gradient and interior-point approaches, respectively. The results demonstrate that the gradient approach has a faster convergence rate than that of the interior-point method and both of them can converge within 30 iterations, which is the result of employing the Armijo rule of backtracking line search.

VII. Conclusion

Comparing with the traditional RadComm system with PA, whose beampattern is only angle-dependent, this work proposed a joint PA and FDA RadComm system, whose beampattern is associated with angle, range and time. The benefits of the proposed scheme, on the one hand, lower the interference between Radar and communications because of fewer overlapped resource blocks between the PA and

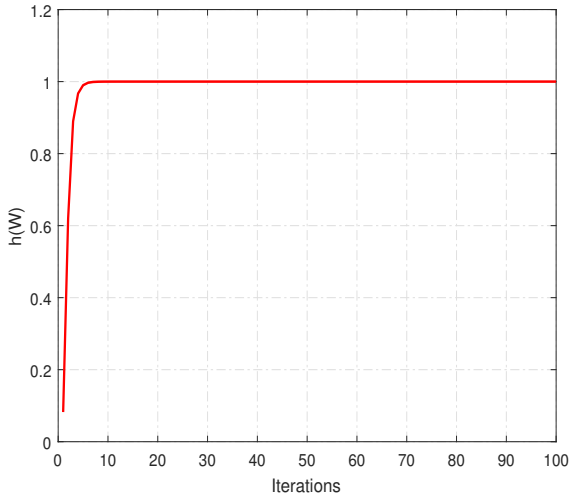

Fig. 13: Convergence rate for the Ratio-Maximizing algorithm using gradient approach.

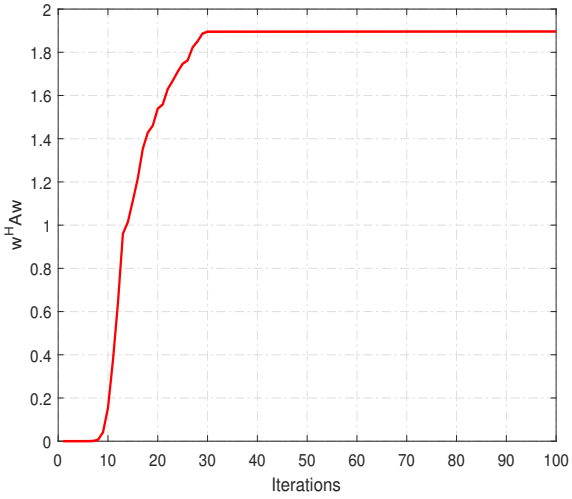

Fig. 14: Convergence rate for the QCQP algorithm using interior-point approach.

FDA antennas; on the other hand, they can share the common CSI and DOA of both the MS and the target, which can reduce the system complexity. To obtain the optimal performance for communications and Radar, we jointly optimized their SINRs under different power split ratios with the Ratio-Maximizing and QCQP methods. In addition, to robustify the proposed algorithm, the case of channel estimation imprecision is considered. At last, we analyzed how the shape of the FDA pulse can be controlled with different factors. Numerical simulations show that the harvested SINR is significantly promoted by the proposed methods compared with the conventional PA scheme.

REFERENCES

[1] S. Sodagari, A. Khawar, T. C. Clancy, and R. McGwier, "A projection based approach for Radar and telecommunications systems coexistence," in *Proc. IEEE Global Commun. Conf. (GLOBECOM)*, Dec. 2012, pp. 5010–5014.

[2] A. Babaei, W. H. Tranter, and T. Bose, "A nullspace-based precoder with subspace expansion for Radar/communications coexistence," in *Proc. IEEE GLOBECOM, Atlanta*, GA, USA, Dec. 2013, pp. 3487–3492.

[3] A. Khawar, A. Abdelhadi, and C. Clancy, "Target detection performance of spectrum sharing MIMO Radars," *IEEE Sensors J.*, vol. 15, no. 9, pp. 4928–4940, Sep. 2015.

[4] A. Khawar, A. Abdelhadi, and T. C. Clancy, "Coexistence analysis between Radar and cellular system in LoS channel," *IEEE Antennas Wireless Propag. Lett.*, vol. 15, pp. 972–975, 2016.

[5] J. A. Mahal, A. Khawar, A. Abdelhadi, and T. C. Clancy, "Spectral coexistence of MIMO Radar and MIMO cellular system," *IEEE Trans. Aerosp. Electron. Syst.*, vol. 53, no. 2, pp. 655–668, Apr. 2017.

[6] F. Liu, C. Masouros, A. Li, H. Sun and L. Hanzo, "MU-MIMO Communications With MIMO Radar: From Co-Existence to Joint Transmission," in *IEEE Transactions on Wireless Communications*, vol. 17, no. 4, pp. 2755-2770, April 2018.

[7] M. Rihan and L. Huang, "Optimum co-design of spectrum sharing between MIMO Radar and MIMO communications systems: An interference alignment approach," *IEEE Transactions on Vehicular Technology*, vol. 62, no. 12, pp. 11667- 11680, Dec. 2018.

[8] P. Kumari, M. E. Eltayeb and R. W. Heath, "Sparsity-aware adaptive beamforming design for IEEE 802.11ad-based joint communications-Radar," *2018 IEEE Radar Conference (RadarConf18)*, Oklahoma City, OK, 2018, pp. 0923-0928.

[9] Y. Liao, H. Tang, W. -Q. Wang and M. Xing, "A Low Sidelobe Deceptive Jamming Suppression Beamforming Method With a Frequency Diverse Array," in IEEE Transactions on Antennas and Propagation, vol. 70, no. 6, pp. 4884-4889, June 2022.

[10] L. Huang, Z. Zong, S. Zhang and W. -Q. Wang, "2-D Moving Target Deception Against Multichannel SAR-GMTI Using Frequency Diverse Array," in IEEE Geoscience and Remote Sensing Letters, vol. 19, pp. 1-5, 2022.

[11] Z. Zhu, W. Chen, Y. Yang and Q. Shu, "Frequency Diverse Array Beampattern Synthesis With Random Permutated Power Increasing Frequency Offset," in IEEE Antennas and Wireless Propagation Letters, vol. 21, no. 10, pp. 1975-1979, Oct. 2022.

[12] Y. Liao, J. Wang and Q. H. Liu, "Transmit Beampattern Synthesis for Frequency Diverse Array With Particle Swarm Frequency Offset Optimization," in IEEE Transactions on Antennas and Propagation, vol. 69, no. 2, pp. 892-901, Feb. 2021.

[13] A. Akkoc, E. Afacan and E. Yazgan, "Dot-Shaped 3D Range-Angle Dependent Beamforming With Discular Frequency Diverse Array," in IEEE Transactions on Antennas and Propagation, vol. 69, no. 10, pp. 6500-6508, Oct. 2021.

[14] Y. Liu, R. Zhu and Q. Liu, "A Novel Low-Cost Frequency Diverse Array With Mirrored Two-Wave Mixing," in IEEE Microwave and Wireless Technology Letters, vol. 33, no. 3, pp. 359-362, March 2023.

[15] C. Im, J. -W. Lee and C. Lee, "Dynamic Energy Beamforming for Multiple IoT Devices With Frequency Diverse Array," in IEEE Internet of Things Journal, vol. 9, no. 15, pp. 13995-14004, 1 Aug.1, 2022.

[16] W. Khan, I. M. Qureshi, and S. Saeed, "Frequency diverse array Radar with logarithmically increasing frequency offset," *IEEE Antennas Wireless Propag. Lett.*, vol. 14, no. 1, pp. 499–502, 2015.

[17] J. Xu, G. Liao, S. Zhu, L. Huang and H. C. So,"Joint Range and Angle Estimation Using MIMO Radar With Frequency Diverse Array," in *IEEE Transactions on Signal Processing*, vol. 63, no. 13, pp. 3396-3410, July 1, 2015.

[18] Q. Li, L. Huang, H. C. So, H. Xue, and P. Zhang,"Beampattern synthesis for FDA-Radar via reweighted - norm iterative phase compensation," *IEEE Transactions on Aerospace and Electronic Systems*, vol. 54, no. 1, pp. 467-475, Feb. 2018.

[19] K. D. Gao, W.-Q. Wang, J. Y. Cai, and J. Xiong, "Decoupled frequency diverse array range-angle-dependent beampattern synthesis using nonlinearly increasing frequency offsets," *IET Microw., Antennas Propag.*, vol. 10, no. 8, pp. 880–884, Aug. 2016.

[20] W. Khan, I. M. Qureshi, A. Basit, and W. Khan, "Range-bins-based MIMO frequency diverse array Radar with logarithmic frequency offset," *IEEE Antennas Wireless Propag. Lett.*, vol. 15, no. 1, pp. 885–888, 2016.

[21] W. Khan and I. M. Qureshi, "Frequency diverse array Radar with timedependent frequency offset," *IEEE Antennas Wireless Propag. Lett.*, vol. 13, no. 1, pp. 758–761, 2014.

[22] S. Han, C. Y. Fan, and X. T. Huang, "Frequency diverse array with timedependent transmit weights," in *Proc. 13th Int. Conf. Signal Process.*, Chengdu, China, Nov. 2016, pp. 448–451.

[23] H. Z. Shao, J. Dai, J. Xiong, H. Chen, and W.-Q. Wang, "Dot-shaped range-angle beampattern synthesis for frequency diverse array," *IEEE Antennas Wireless Propag. Lett.*, vol. 15, no. 1, pp. 1703–1706, 2016.

[24] Y. M. Liu, R. Hang, L. Wang, and A. Nehorai, "The random frequency diverse array: A new antenna structure for uncoupled direction-range direction in active sensing," *IEEE J. Sel. Topics Signal Process.*, vol. 11, no. 2, pp. 295–308, Mar. 2017.

[25] W. Wang, "Retrodirective Frequency Diverse Array Focusing for Wireless Information and Power Transfer," in *IEEE Journal on Selected Areas in Communications*, vol. 37, no. 1, pp. 61-73, Jan. 2019.

[26] S. Qin, Y. D. Zhang, M. G. Amin, and F. Gini, "Frequency diverse coprime arrays with coprime frequency offsets for multitarget localization," *IEEE J. Sel. Topics Signal Process.*, vol. 11, no. 2, pp. 321–335, Mar. 2017.

[27] Y. H. Xu, X.W. Shi,W. T. Li, and J.W. Xu, "Flat-top beampattern synthesis in range and angle domains for frequency diverse array via second-order cone programming," *IEEE Antennas Wireless Propag. Lett.*, vol. 15, no. 1, pp. 1479–1482, 2016.

[28] A.-M. Yao, W. Wu, and D.-G. Fang, "Frequency diverse array antenna using time-modulated optimized frequency offset to obtain time-invariant spatial fine focusing beampattern," *IEEE Transactions on Antennas and Propagation*, vol. 64, no. 10, pp. 4434–4446, October 2016.

[29] A.-M. Yao, W. Wu, and D.-G. Fang, "Solutions of time-invariant spatial focusing for multi-targets using time modulated frequency diverse arrays," *IEEE Transactions on Antennas and Propagation*, vol. 65, no. 2, pp. 552–566, February 2017.

[30] Y.-Q. Yang, H. Wang, H.-Q. Wang, S.-Q. Gu, D.-L. Xu, and S.-L. Quan, "Optimization of sparse frequency diverse array with time-invariant spatial-focusing beampattern," *IEEE Antennas and Wireless Propagation Letters*, vol. 17, no. 2, pp. 351–354, February 2018.

[31] Qin, Si., "Coprime Signal Processing for Spatial and Temporal Spectrum Sensing," *Villanova University*, pp. 108-127, 2016.

[32] Boyd, Stephen, and Lieven Vandenberghe, "Convex optimization," *Cambridge university press*, pp.464-466, 2004.

[33] P. Smulders and L. Correia, "Characterisation of propagation in 60 GHz radio channels," *Electronics and Communication Engineering Journal*, vol. 9, no. 2, pp. 73–80, 1997.

[34] H. Xu, V. Kukshya, and T. Rappaport, "Spatial and temporal characteristics of 60-GHz indoor channels," *IEEE Journal on Selected Areas in Communications*, vol. 20, no. 3, pp. 620–630, 2002.

[35] E. Ben-Dor, T. Rappaport, Y. Qiao, and S. Lauffenburger, "Millimeterwave 60 GHz outdoor and vehicle AOA propagation measurements using a broadband channel sounder," in *IEEE Global Telecommunications Conference*, 2011, pp. 1–6.

[36] Q. Spencer, B. Jeffs, M. Jensen, and A. Swindlehurst, "Modeling the statistical time and angle of arrival characteristics of an indoor multipath channel," *IEEE Journal on Selected Areas in Communications*, vol. 18, no. 3, pp. 347–360, 2000.

[37] A. Sayeed and V. Raghavan, "Maximizing MIMO capacity in sparse multipath with reconfigurable antenna arrays," *IEEE Journal of Selected Topics in Signal Processing*, vol. 1, no. 1, pp. 156–166, 2007.

[38] F. Paisana, G. A. Ropokis, N. Marchetti and L. A. DaSilva, "Cognitive Beamforming in Radar Bands," in IEEE Transactions on Communications, vol. 66, no. 8, pp. 3623-3637, Aug. 2018.

[39] Z. Luo, W. Ma, A. M. So, Y. Ye and S. Zhang, "Semidefinite Relaxation of Quadratic Optimization Problems," in IEEE Signal Processing Magazine, vol. 27, no. 3, pp. 20-34, May 2010.

Freddy Y.P. Feng received his M.A.Sc degree in Electrical Engineering from Nanjing University of Information Science and Technology (NUIST) in Nanjing, China in 2014. He went on to earn his Ph.D in Electrical Engineering from Pusan National University (PNU) in Busan, South Korea in 2018. From May to August 2018, he was a visiting scholar at the University of Melbourne in Victoria, Australia. Following his Ph.D, he worked as a postdoctoral fellow in the College of Information Engineering at Shenzhen University from November 2018 to 2021. Since 2021, he has been an Assistant Professor at the Shenzhen Institute of Information Technology. His research interests span millimeter wave communications, signal processing, compressive sensing, mathematical optimization, and machine learning.

Suk Chan Kim (Senior Member, IEEE) received the B.S.E. degree (summa cum laude) in electronics engineering from Pusan National University (PNU), Busan, South Korea, in February 1993, and the M.S.E. and Ph.D. degrees in electrical engineering from the Korea Advanced Institute of Science and Technology (KAIST), Daejeon, South Korea, in February 1995 and 2000, respectively. He has been a Professor with the Department of Electronics Engineering, PNU, since 2002. His current research interests include mobile communications, statistical signal processing, and applied machine learning for healthcare and communications. He is a member of the Institute of Electronics Engineers of Korea (IEEK) and the Korean Institute of Communication Sciences (KICS). He received the Haedong Paper Award from KICS, in 2005.

Ziming He is currently the Director of R&D and a Principal Scientist with Zhejiang Vie Science & Technology Co., Ltd. His research interests include navigation and communication for electric vehicle wireless charging and autonomous vehicles. He is the inventor of 20+ granted/pending patents.

Feng Chen is currently the Chairman and General Manager with Zhejiang Vie Science & Technology Co., Ltd. He has won many honorary titles such as "Outstanding Entrepreneur in China's Machinery Industry" and "Top Ten People in China's Automotive Parts Industry in 2008", etc.

Chen Lu received a Ph.D. degree from Xi'an Jiaotong University, Xi'an, in 2004. He is currently a Professor with the School of Information and Communication, Shenzhen Institute of Information Technology. His research interests include space-air-ground-water integrated communications, network security, digital health, future media etc. He is the Winner of the China Invention Patent Gold Award and Excellence Award and the Guangdong Invention Patent Gold Award.

Sami Muhaidat (Senior Member, IEEE) received the Ph.D. degree in Electrical and Computer Engineering from the University of Waterloo, Waterloo, ON, Canada, in 2006. He is currently a Professor and the Deputy Director of the 6G Research Center at Khalifa University, Abu Dhabi, UAE, and an Adjunct Professor with Carleton University, Ontario, Canada. He is also a Visiting Reader with the Faculty of Engineering, University of Surrey, Guildford, U.K. His research interests focus on advanced digital signal processing techniques for wireless communications, intelligent surfaces, MIMO, optical communications, massive multiple access techniques, backscatter communications, and machine learning for communications. He is currently an Area Editor of the IEEE Transactions on Communications, a Guest Editor of the IEEE Network "Native Artificial Intelligence in Integrated Terrestrial and Non-Terrestrial Networks in 6G" special issue, and a Guest Editor of the IEEE OJVT "Recent Advances in Security and Privacy for 6G Networks" special issue. He served as a Senior Editor and Editor of the IEEE Communications Letters, an Editor of the IEEE Transactions on Communications, and an Associate Editor of the IEEE Transactions on Vehicular Technology.